Research Article | Vol. 28, No. 15 / 20 July 2020 / Optics Express 21729

Optics EXPRESS

Standing wave polarization holography for realizing liquid crystal Pancharatnum-Berry phase lenses

ZIQIAN HE,[1,2] KUN YIN,[1,2] AND SHIN-TSON WU[1,*]

[1]College of Optics and Photonics, University of Central Florida, Orlando, FL 32816, USA
[2]These authors contributed equally to this work
[*]swu@creol.ucf.edu

Abstract: A standing wave polarization holography setup is proposed to generate the desired polarization field for fabricating both on-axis and off-axis liquid crystal Pancharatnum-Berry phase lenses. Compared to other interference exposure setups, standing wave interferometry can double the polarization field amplitude because it does not require a beam splitter. Moreover, the optical axis angle of the lenses can be easily adjusted without realigning the optical setup. Based on the design, we first theoretically derive the polarization field distribution. In the experiment, we build the recording optical system and fabricate a series of on-axis and off-axis lenses. Further optical characterization proves the high diffraction efficiency of the fabricated lenses.

© 2020 Optical Society of America under the terms of the OSA Open Access Publishing Agreement

1. Introduction

Recent advances of Pancharatnum-Berry (PB) phase (also termed geometric phase) optical elements based on liquid crystals (LCs) have drawn great research interest [1,2]. In contrast to traditional dynamic phase produced via optical path difference, PB phase is generated by the changes in other parameters of light. A well-known way of introducing PB phase is through spin flip. This can be achieved by patterning LCs with half-wave thickness (transmissive type) or cholesteric liquid crystals (CLCs, reflective type). Through 180° rotation of LC alignment direction, a full 2π phase change can be mapped. Utilizing this principle, a variety of diffractive optical elements can be obtained by patterning LCs [1,2]. Such optical elements have also found a wide range of applications, such as laser beam steering [3–7], optical communication [8], polarimetry [9], thin-film polarizers [10] and near-to-eye displays [11–15].

To enable these LC-based PB phase optical elements, an effective method of patterning LC alignment direction is pivotal. Thanks to the rapid progress of optical materials and micro-fabrication technologies, several methods have been demonstrated, including interferometry [16–18], direct laser recording [19], projection lithography [20,21], and nanoimprinting [22]. Except nanoimprinting, other methods are all based on photoalignment materials. Among them, interferometry-based methods are commonly used to create PB gratings and lenses with continuous phase distribution, which also means high optical quality. While most interferometry methods involve at least one beam splitter (BS), standing wave interferometry is a unique class that does not need a BS to split the input beam into two optical paths, and thus should result in the highest intensity of the recording polarization field. Moreover, it has been previously shown that the photoalignment pattern of PB gratings having different diffraction angles can be easily realized by rotating the sample with respect to the optical axis of the recording optical system [23]. There is no need to realign the recording optical system.

In this paper, the recording method of standing wave polarization holography is further generalized. An interference exposure recording system is proposed to achieve the polarization field for both on-axis and off-axis PB lenses. We begin with theoretically calculating the polarization field distribution. Then, we establish the recording optical system and show the

#399036 https://doi.org/10.1364/OE.399036
Journal © 2020 Received 1 Jun 2020; revised 27 Jun 2020; accepted 28 Jun 2020; published 7 Jul 2020

Optics EXPRESS

effectiveness of the setup by fabricating these on-axis and off-axis PB lenses. Further optical characterization proves that PB lenses with decent quality can be obtained. The proposed optical setup is particularly useful for fabricating PB lenses with different optical axis angles, which have shown promising applications in off-axis optical systems and folded optical-path systems, such as compact spectroscopy [24].

2. Standing wave polarization holography for PB lenses

The optical setup of standing wave polarization holography for PB lenses is schematically plotted in Fig. 1(a). The incoming (orange color) collimated circularly polarized laser beam, which can be either right-handed circularly polarized (RCP) or left-handed circularly polarized (LCP), passes through the glass substrate coated with photoalignment materials, and is reflected by the reflective lens with polarization management. More specifically, the reflective lens has two functions: converging the incoming beam and flipping its polarization. For this part, many combinations of optical components can fulfil this functionality. Here, three examples are shown in Fig. 1(a). A mirror-lens-quarter-wave plate (QWP) stack can import power to the incoming beam and flip the circular polarization. Equivalently, a reflective lens (curved mirror) can replace the mirror-lens stack, or a single reflective CLC lens can accomplish both functions [25]. Upon reflection, the reflected beam (green color) passes through the photoalignment layer and a polarization field is created on such a layer. From Fig. 1(a), the photoalignment layer is placed at approximately $2f$ from the reflective lens part, where f (=25 cm) is the effective focal length of the reflective lens, and the photoalignment layer can be rotated in reference to the optical axis of the exposure setup.

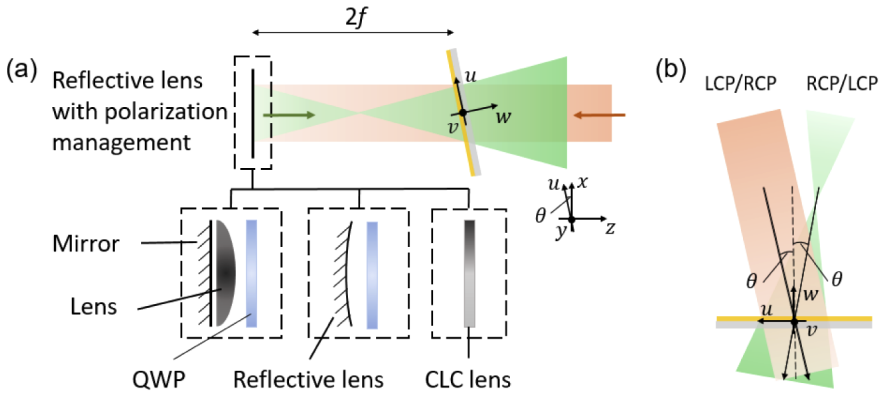

Fig. 1. (a) Schematic of proposed standing wave polarization holography setup, in which the reflective lens part can have a variety of choices as depicted. (b) An equivalent form of the exposure setup.

If we assign a global coordinate system (xyz) to the exposure setup and a local coordinate system (uvw) to the photo-alignment layer as shown in Fig. 1(a), the recorded polarization field can be derived as a function of θ (i.e. the angle between u and x axes). The phase distribution of the incoming beam (φ_r) has a paraxial form of:

$$\varphi_r = \frac{2\pi}{\lambda}\theta u, \tag{1}$$

where λ is the recording wavelength in air. On the other hand, the phase distribution of the reflected beam (φ_l) has the form of a diverging off-axis lens as:

$$\varphi_l = \frac{2\pi}{\lambda}\left(\sqrt{f^2\cos^2\theta + (u - f\sin\theta)^2 + v^2} - f\right). \tag{2}$$

Optics EXPRESS

Its paraxial form can be approximated as:

$$\varphi_l = \frac{\pi}{\lambda f}(u^2 + v^2) - \frac{2\pi}{\lambda}\theta u. \tag{3}$$

Considering that the incoming beam and the reflected beam have different handedness but nearly equal amplitude, the polarization field generated on the photoalignment layer can be derived as:

$$E = \begin{bmatrix} 1 \\ \pm i \end{bmatrix} e^{i\varphi_r} + \begin{bmatrix} 1 \\ \mp i \end{bmatrix} e^{i\varphi_l} = 2e^{i\frac{\pi}{2\lambda f}(u^2+v^2)} \begin{bmatrix} \cos\left(\frac{\pi}{2\lambda f}(u^2 + v^2) - \frac{2\pi}{\lambda}\theta u\right) \\ \mp \sin\left(\frac{\pi}{2\lambda f}(u^2 + v^2) - \frac{2\pi}{\lambda}\theta u\right) \end{bmatrix}. \tag{4}$$

The field is linearly polarized, and the linear polarization continuously rotates in the uv plane. The plus and minus signs represent different rotation direction (clockwise and counterclockwise) of the linear polarization. From here, we can see that our proposed optical setup is equivalent to the optical setup shown in Fig. 1(b), which is the traditional polarization holography setup for off-axis PB lenses [26]. In a traditional polarization holography setup, when the off-axis angle changes, the entire system needs to be realigned to ensure that the two beams coincide at the photoalignment layer. However, in our setup, the off-axis angles can be easily tuned by rotating the substrate. If an LC layer with half-wave thickness is coated onto the substrate, circularly polarized light passing through such an LC device will be imposed a PB phase term as:

$$\varphi_{PBL} = \pm i\left(\frac{\pi}{\lambda f}(u^2 + v^2) - \frac{4\pi}{\lambda}\theta u\right). \tag{5}$$

This is an off-axis lens in paraxial form with a focal length of $\pm f$ (depending on the handedness of light) and an off-axis angle of 2θ. The on-axis lenses can also be obtained by simply setting $\theta = 0°$.

3. Results and discussion

3.1. Sample fabrication

To demonstrate feasibility, the proposed standing wave polarization holography setup is established and a mirror-lens-QWP stack is employed as the reflective lens part. The focal length of the lens is ~50 cm and the distance between the mirror and the lens is ~1.3 cm. The substrate holder is placed at ~46 cm away from the lens to ensure a similar electric field amplitude for both incoming and reflected beams. An OBIS 488-nm LS 60-mW laser from Coherent is employed as the exposure source.

To fabricate PB lenses, first a thin film of the photoalignment material, 0.4wt% Brilliant Yellow (BY, from Tokyo Chemistry Industry) dissolved in dimethylformamide (DMF) solvent, is spin-coated onto cleaned glass substrates with 500 rpm for 5 s and 3000 rpm for 30 s. Then, the substrates coated with BY are mounted on the sample holder for exposure, with a dosage of ~1.2 J/cm^2 (2 min with ~9.9 mW/cm^2 irradiance). In experiment, 6 samples are exposed, with the off-axis angles (θ) of approximately 0°, 1°, 2°, 3°, 4°, 5°. The diameter of the exposed aperture is about 9 mm. After exposure, a reactive mesogen solution, consisting of 99wt% reactive mesogen RM257 (from LC Matter) and 1wt% photo initiator Irgacure 651 (from BASF) dissolved in toluene with a weight ratio of 1:3, is spin-coated onto the substrates with 2000 rpm for 30 s. As the final step, the samples are cured by a UV light (365 nm) for 5 min with ~10 mW/cm^2 irradiance. Here passive devices based on LC polymers are fabricated for illustration. In general, active devices can also be fabricated by assembling a LC cell with the exposed substrates and filling with LCs.

Optics EXPRESS

3.2. Sample characterization

Polarized optical microscope (POM, OLYMPUS BX51) images of an off-axis lens ($\theta = 2°$) are captured as shown in Fig. 2. Figures 2(a) and 2(b) are captured near the center and the edge of the lens, respectively. For both regions, the fringes can be clearly discerned. The central part of the lens is quite clear, while the peripheral region shows tiny alignment defects, which are closely related to the quality of the template lens employed for exposure.

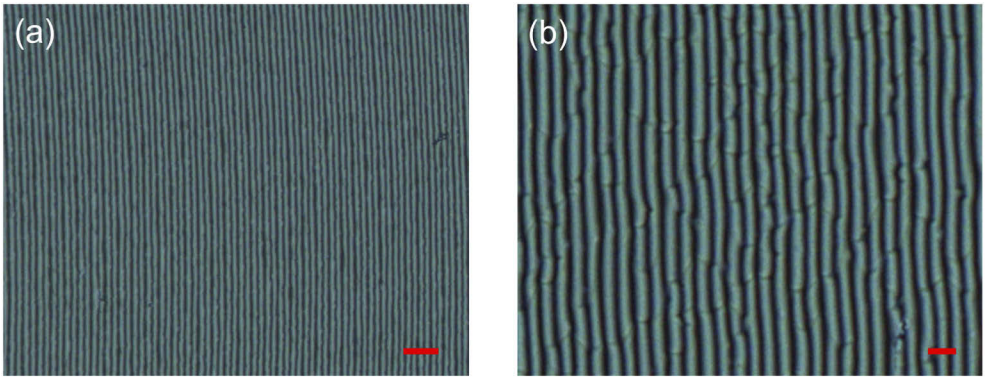

Fig. 2. POM images taken near (a) the center and (b) the edge of an off-axis PB lens with $\theta = 2°$. Scale bar: (a) 50 μm and (b) 10 μm.

The spectral property of an off-axis lens ($\theta = 4°$) sample is also characterized, using an Ocean Optics spectrometer (HR4000CG-UV-NIR). With the fabricated lens sandwiched in between two broadband circular polarizers, the transmission spectrum is recorded as Fig. 3 shows. The minimum transmittance is located at ~513 nm, corresponding to the wavelength that fulfils half wave condition. It indicates that the wavelength of highest diffraction efficiency should be at ~513 nm for this lens.

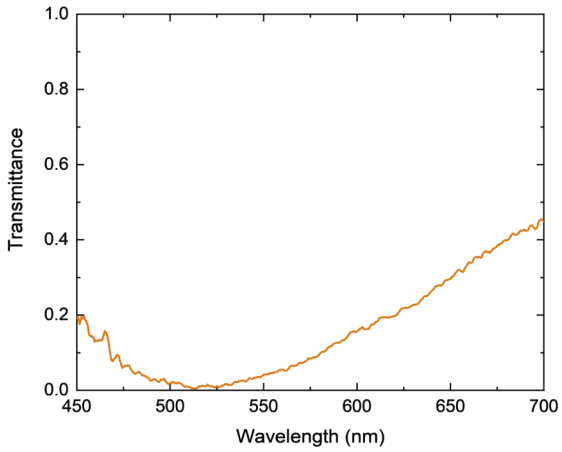

Fig. 3. Transmission spectrum measured by inserting an off-axis lens ($\theta = 4°$) in between two broadband circular polarizers.

To further characterize the diffraction efficiency of the lenses and show the lensing effect, an expanded 532-nm laser beam (from a laser diode) is employed to shine upon the lenses and a black screen is placed at ~37 cm away from the lenses. A linear polarizer and a QWP are

Optics EXPRESS

placed in front of the laser to control its polarization. The setup is shown in Fig. 4(a). The intensity of each diffraction order is recorded utilizing a power meter. The diffraction patterns are shown in Fig. 4(b). While the −1-diffraction order is diverging the laser beam, the + 1-diffraction order is converging. The diffraction angle increases as the rotation angle θ increases. The efficiency of the ± 1 diffraction orders can also be varied by tuning the incident polarization. With RCP input light, the + 1-diffraction order manifests the highest diffraction efficiency, while the diffraction efficiency reaches the peak for the −1-diffraction order when the input light is LCP. The quantitative diffraction efficiency of all the cases are summarized in Table 1. For the off-axis lenses with $\theta = 3°$, 4° and 5°, their first order diffraction efficiency (for a circularly polarized light) all exceeds 90%, which ensures the good quality of lenses. The efficiency of the lenses with $\theta = 1°$ and 2° is slightly lower (but still over 87%), which might be caused by the deviation of LC layer thickness from the half-wave and some other fabrication errors. The diffraction efficiency of the on-axis lens with RCP input is also measured by filtering out other orders using an iris.

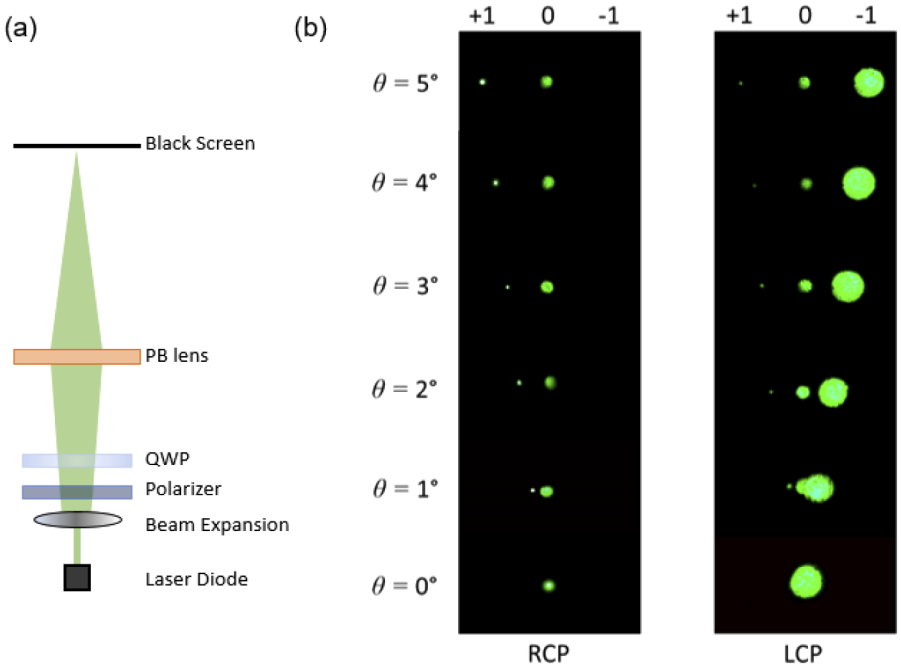

Fig. 4. (a) Measurement setup. (b) Diffraction patterns generated by a series of PB lenses with different optical axis angles. The images on the left column are with right-handed circularly polarized (RCP) input light, while those on the right column are with left-handed circularly polarized (LCP) input light.

3.3. Discussion

Beside the exposure setup used in this work, there are other variations, which can lead to a slightly different formula of the generated polarization field. One example is shown in Fig. 5(a). Here two lenses are applied in the setup. Ideally, the reflected beam will coincide with the incoming beam, and the substrate coated with photoalignment layer can be placed anywhere in between the two lenses. In this case, the polarization field on the photoalignment layer can be described as:

$$E = 2\begin{bmatrix} \cos\left(\frac{\pi}{\lambda f_1}(u^2+v^2) - \frac{2\pi}{\lambda}\theta u\right) \\ \mp\sin\left(\frac{\pi}{\lambda f_1}(u^2+v^2) - \frac{2\pi}{\lambda}\theta u\right) \end{bmatrix}, \tag{6}$$

Optics EXPRESS

Table 1. Diffraction efficiency distribution of the fabricated off-axis lenses.

	RCP input			LCP input		
θ	+1 order	0 order	−1 order	+1 order	0 order	−1 order
0°	95.1%	4.6%	0.3%	-	-	-
1°	88.1%	11.4%	0.5%	2.6%	10.2%	87.2%
2°	88.8%	10.4%	0.8%	1.9%	8.8%	89.3%
3°	92.5%	6.7%	0.8%	2.0%	5.9%	92.1%
4°	94.6%	4.5%	0.9%	1.2%	3.7%	95.1%
5°	92.9%	6.8%	0.3%	2.1%	6.1%	91.8%

where f_1 is the distance between the center of the substrate and the focal plane of the lens. The equivalent form of this exposure setup is illustrated in Fig. 5(b).

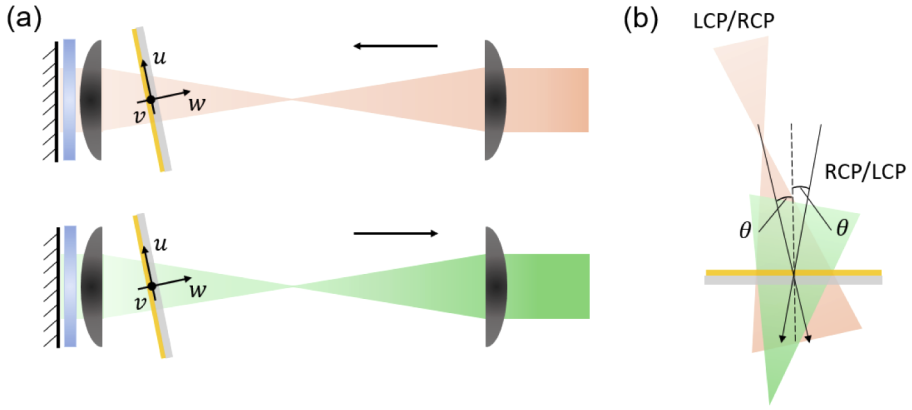

Fig. 5. (a) Schematic of a variation standing wave polarization holography setup, where the reflected beam coincides with the incident beam. (b) An equivalent form of the exposure setup.

Another important aspect of our proposed setup is the field amplitude matching between the incoming beam and the reflected beam, as the equation describing the polarization field is derived with equal amplitude. Although there is some tolerance if the amplitude of both beams is not equal (our experiments show a tolerance of about ± 10% intensity difference), it would be better to reduce this amplitude difference as small as possible. In our case, the photoalignment layer is facing toward the lens and there is no anti-reflection coating on the substrate as well as on the lens. Thus, the electric field amplitude of the reflected beam will decrease due to reflection (~4% intensity loss each time) upon each air/glass interface. Here, this issue is resolved by placing the substrate closer to the lens. Given that the effective focal length (f) of the composite reflective lens is ~25 cm, ideally the substrate should be positioned at ~50 cm ($2f$). In our experiment, the distance is ~46 cm instead. Apparently, another method to eliminate this kind of influence is by applying anti-reflection coatings to the surfaces.

4. Conclusion

In conclusion, a standing wave polarization holography setup has been proposed to generate the desired polarization field for fabricating both on-axis and off-axis PB lenses. Based on the design, we theoretically derived the polarization field distribution. In experiments, we constructed the recording optical system and successfully fabricated a series of on-axis and off-axis PB lenses.

Optics EXPRESS

Further optical characterization proved the high diffraction efficiency of the fabricated PB lenses. Comparing to traditional interference exposure setup, our proposed setup is particularly useful for manufacturing PB lenses with different optical axis angles.

Funding

Air Force Office of Scientific Research (FA9550-14-1-0279).

Disclosures

The authors declare no conflicts of interest.

References

1. T. Zhan, Y. H. Lee, G. Tan, J. Xiong, K. Yin, F. Gou, J. Zou, N. Zhang, D. Zhao, J. Yang, S. Liu, and S. T. Wu, "Pancharatnam-Berry optical elements for head-up and near-eye displays," J. Opt. Soc. Am. B **36**(5), D52–D65 (2019).
2. P. Chen, B.-Y. Wei, W. Hu, and Y.-Q. Lu, "Liquid-crystal-mediated geometric phase: from transmissive to broadband reflective planar optics," Adv. Mater. 1903665 (2019).
3. Z. He, F. Gou, R. Chen, K. Yin, T. Zhan, and S. T. Wu, "Liquid Crystal Beam Steering Devices: Principles, Recent Advances, and Future Developments," Crystals **9**(6), 292 (2019).
4. J. Kim, C. Oh, S. Serati, and M. J. Escuti, "Wide-angle, nonmechanical beam steering with high throughput utilizing polarization gratings," Appl. Opt. **50**(17), 2636–2639 (2011).
5. K. Yin, Y. H. Lee, Z. He, and S. T. Wu, "Stretchable, flexible, rollable, and adherable polarization volume grating film," Opt. Express **27**(4), 5814–5823 (2019).
6. F. Gou, F. Peng, Q. Ru, Y. H. Lee, H. Chen, Z. He, T. Zhan, K. L. Vodopyanov, and S. T. Wu, "Mid-wave infrared beam steering based on high-efficiency liquid crystal diffractive waveplates," Opt. Express **25**(19), 22404–22410 (2017).
7. J. Kim, M. N. Miskiewicz, S. Serati, and M. J. Escuti, "Nonmechanical laser beam steering based on polymer polarization gratings: Design optimization and demonstration," J. Lightwave Technol. **33**(10), 2068–2077 (2015).
8. P. Chen, L. L. Ma, W. Duan, J. Chen, S. J. Ge, Z. H. Zhu, M. J. Tang, R. Xu, W. Gao, T. Li, W. Hu, and Y. Q. Lu, "Digitalizing Self-Assembled Chiral Superstructures for Optical Vortex Processing," Adv. Mater. **30**(10), 1705865 (2018).
9. M. W. Kudenov, M. J. Escuti, N. Hagen, E. L. Dereniak, and K. Oka, "Snapshot imaging Mueller matrix polarimeter using polarization gratings," Opt. Lett. **37**(8), 1367–1369 (2012).
10. T. Du, F. Fan, A. M. W. Tam, J. Sun, V. G. Chigrinov, and H. S. Kwok, "Complex nanoscale-ordered liquid crystal polymer film for high transmittance holographic polarizer," Adv. Mater. **27**(44), 7191–7195 (2015).
11. Y. H. Lee, T. Zhan, and S. T. Wu, "Enhancing the resolution of a near-eye display with Pancharatnam−Berry phase deflector," Opt. Lett. **42**(22), 4732–4735 (2017).
12. T. Zhan, Y. H. Lee, and S. T. Wu, "High-resolution additive light field near-eye display by switchable Pancharatnam–Berry phase lenses," Opt. Express **26**(4), 4863–4872 (2018).
13. G. Tan, Y. H. Lee, T. Zhan, J. Yang, S. Liu, D. F. Zhao, and S. T. Wu, "Foveated imaging for near-eye displays," Opt. Express **26**(19), 25076–25085 (2018).
14. C. Yoo, K. Bang, M. Chae, and B. Lee, "Extended-viewing-angle waveguide near-eye display with a polarization-dependent steering combiner," Opt. Lett. **45**(10), 2870–2873 (2020).
15. K. Yin, H. Y. Lin, and S. T. Wu, "Chirped polarization volume grating with ultra-wide angular bandwidth and high efficiency for see-through near-eye displays," Opt. Express **27**(24), 35895–35902 (2019).
16. K. Gao, H.-H. Cheng, A. K. Bhowmik, and P. J. Bos, "Thin-film Pancharatnam lens with low f-number and high quality," Opt. Express **23**(20), 26086–26094 (2015).
17. T. Zhan, J. Xiong, Y. H. Lee, and S. T. Wu, "Fabrication of Pancharatnam-Berry phase optical elements with highly stable polarization holography," Opt. Express **27**(3), 2632–2642 (2019).
18. J. Xiong, T. Zhan, and S. T. Wu, "A versatile method for fabricating Pancharatnam-Berry micro-optical elements," Opt. Express **27**(20), 27831–27840 (2019).
19. J. Kim, Y. Li, M. N. Miskiewicz, C. Oh, M. W. Kudenov, and M. J. Escuti, "Fabrication of ideal geometricphase holograms with arbitrary wavefronts," Optica **2**(11), 958–964 (2015).
20. M. Jiang, Y. Guo, H. Yu, Z. Zhou, T. Turiv, O. D. Lavrentovich, and Q.-H. Wei, "Low F-number diffraction-limited Pancharatnam-Berry microlenses enabled by plasmonic photopatterning of liquid crystal polymers," Adv. Mater. **31**(18), 1808028 (2019).
21. Y. Li, Y. Liu, S. Li, P. Zhou, T. Zhan, Q. Chen, Y. Su, and S. T. Wu, "Single-exposure fabrication of tunable Pancharatnam-Berry devices using a dye- doped liquid crystal," Opt. Express **27**(6), 9054–9060 (2019).
22. Z. He, Y. H. Lee, R. Chen, D. Chanda, and S. T. Wu, "Switchable Pancharatnam-Berry microlens array with nano-imprinted liquid crystal alignment," Opt. Lett. **43**(20), 5062–5065 (2018).

Optics EXPRESS

23. J. P. Vernon, S. V. Serak, R. S. Hakobyan, A. K. Aleksanyan, V. P. Tondiglia, T. J. White, T. J. Bunning, and N. V. Tabiryan, "Recording polarization gratings with a standing spiral wave," Appl. Phys. Lett. **103**(20), 201101 (2013).
24. M. Khorasaninejad, W. T. Chen, J. Oh, and F. Capasso, "Super-dispersive off-axis meta-lenses for compact high resolution spectroscopy," Nano Lett. **16**(6), 3732–3737 (2016).
25. J. Kobashi, H. Yoshida, and M. Ozaki, "Planar optics with patterned chiral liquid crystals," Nat. Photonics **10**(6), 389–392 (2016).
26. K. Yin, Z. He, and S. T. Wu, "Reflective polarization volume lens with small f-number and large diffraction angle," Adv. Opt. Mater. **8**(11), 2000170 (2020).

142.196.250.150 {ts '2020-07-07 21:23:11'}